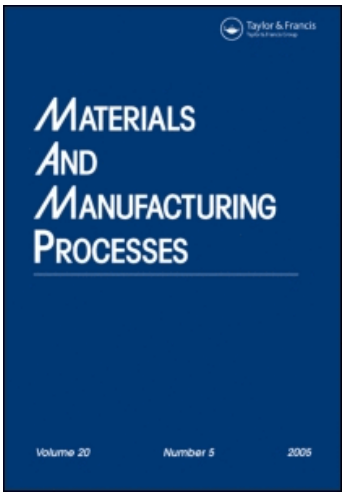

Materials and Manufacturing Processes
Publication details, including instructions for authors and subscription information:
http://www.informaworld.com/smpp/title~content=t713597284

Densification, Microstructure, and Electrical Properties of $BaTiO_3$ (BT) Ceramics Prepared from Ultrasonically De-Agglomerated BT Powders

Smilja Markovi [a]; Miroslav Miljkovi [b]; edomir Jovaleki [c]; Slavko Mentus [d]; Dragan Uskokovi [a]
[a] Institute of Technical Sciences of the Serbian Academy of Sciences and Arts, Belgrade, Serbia [b] Laboratory for Electron Microscopy, Faculty of Medicine, University of Niš, Niš, Serbia [c] Department of Material Science, Institute for Multidisciplinary Research, Belgrade, Serbia [d] Faculty of Physical Chemistry, University of Belgrade, Belgrade, Serbia

Online Publication Date: 01 October 2009

To cite this Article Markovi, Smilja, Miljkovi, Miroslav, Jovaleki, edomir, Mentus, Slavko and Uskokovi, Dragan(2009)'Densification, Microstructure, and Electrical Properties of $BaTiO_3$ (BT) Ceramics Prepared from Ultrasonically De-Agglomerated BT Powders',Materials and Manufacturing Processes,24:10,1114 — 1123
To link to this Article: DOI: 10.1080/10426910903031750
URL: http://dx.doi.org/10.1080/10426910903031750

Materials and Manufacturing Processes, 24: 1114–1123, 2009

ISSN: 1042-6914 print/1532-2475 online
DOI: 10.1080/10426910903031750

Taylor & Francis
Taylor & Francis Group

Densification, Microstructure, and Electrical Properties of $BaTiO_3$ (BT) Ceramics Prepared from Ultrasonically De-Agglomerated BT Powders

Smilja Marković[1], Miroslav Miljković[2], Čedomir Jovalekić[3], Slavko Mentus[4], and Dragan Uskoković[1]

[1]*Institute of Technical Sciences of the Serbian Academy of Sciences and Arts, Belgrade, Serbia*
[2]*Laboratory for Electron Microscopy, Faculty of Medicine, University of Niš, Niš, Serbia*
[3]*Department of Material Science, Institute for Multidisciplinary Research, Belgrade, Serbia*
[4]*Faculty of Physical Chemistry, University of Belgrade, Belgrade, Serbia*

In this study, a correlation between densification, microstructure, and electrical properties of $BaTiO_3$ (BT) ceramics prepared from ultrasonically de-agglomerated BT powders has been analyzed. BT powders with the same crystal structure (tetragonal) and stoichiometry, but with different average particle size, were used to prepare sintered ceramics. Densification and electrical properties of the sintered BT ceramics were correlated to the average particle size of the powders. It was found that a decrease in average particle size improved the densification process as well as the ceramics' microstructure. The impedance measurements were done up to 320°C in order to separate grain (bulk) and grain boundary contributions. Bulk resistance was more or less the same, independent on the average particle size of the powder. On the contrary, grain boundary resistance increased with decreasing average particle size of the powder.

Keywords Barium titanate; Dielectric permittivity; Grain boundary resistance; Microstructure; Shrinkage; Sintering.

1. Introduction

Due to its outstanding dielectric properties and high thermal stability, barium titanate (BT) is widely used in the fabrication of electronic devices such as multilayer ceramic capacitors (MLCCs), positive temperature coefficient of resistance (PTCR) thermistors, piezoelectric sensors, transducers, etc. [1, 2]. Since the 1950s, when Känzig [3] published a theoretical article concerning the dependence of dielectric properties of $BaTiO_3$ on particle size, the influence of the characteristics of starting powders on the properties of the final ceramics has been intensively studied [4–8]. It has been found that nano-sized barium titanate powder with a high tetragonality [9] and a narrow particle size distribution [10, 11] is required for the preparation of dense ceramics with excellent dielectric properties. Therefore, many chemical routes, including coprecipitation [12], hydrothermal synthesis [13], sol-gel synthesis [14], alkoxide hydrolysis [15], citrate routes [16], and ultrasonic spray-pyrolysis [17] have been developed to prepare ultrafine, sintering reactive $BaTiO_3$ powders. Despite the fact that BT powders synthesized in the above-cited processes have nano-sized particles, their tetragonality is often lower. This in turn results in poor dielectric properties. Low tetragonality is attributed to two factors: size effects and hydroxyl ion effect [18]. Tetragonal barium titanate can be prepared by a solid-state reaction between $BaCO_3$ and TiO_2 at the temperature interval of 1000–1200°C [19]. But BT powder prepared at a high temperature exhibits some drawbacks, such as a large particle size (2–5 μm), inhomogeneous mixing, or broad particle size distribution, which generally limits the ability to fabricate reliable electronic components. The sinterability of these powders can be improved by reducing particle size and narrowing particle size distribution, e.g., by mechanical milling of wet powders [20–23]. However, an intensive milling of $BaTiO_3$ in the presence of water may lead to the leaching of Ba^{2+} and a strong pH increase, which may be detrimental for the further processing. Also, during mechanical milling, impurities can be introduced into the system [24]. Instead of mechanical milling, high-intensity ultrasound irradiation (ultrasonication) can be used for the de-agglomeration and activation of powders synthesized by solid-state reaction, thus avoiding the introduction of impurities. Previously, nano-sized BT powder with tetragonal crystal structure was prepared by a solid-state reaction followed by high-intensity ultrasonication during three hours [25].

Barium titanate ceramics contain electro-active intragranular (bulk) and intergranular (grain-boundary) regions, whose properties depend on the microstructure. In many electroceramic applications grain boundaries play an important or even a key functional role [26, 27]. In a broad range of ceramics, this shows ionic, mixed ionic-electronic, or electronic conduction, grain boundaries act as barriers for the cross transport of charge carriers. Often, the barrier character of the grain boundary is especially pronounced in the low temperature regime.

Received October 13, 2008; Accepted January 14, 2009
Address correspondence to Smilja Marković, Institute of Technical Sciences of the Serbian Academy of Sciences and Arts, Knez Mihailova 35/IV, Belgrade 11001, Serbia; E-mail: Smilja.Markovic@itn.sanu.ac.rs

In this regime $BaTiO_3$ is employed as a high permittivity dielectric for capacitor applications. At high temperatures these resistive grain boundary barriers are reduced, giving rise to substantially field-enhanced leakage currents through the components. That is the reason why detailed dielectric studies, especially those concerning grain boundary barriers, are important for full insight into the characteristics of BT. One of the most important methods to investigate the electrical properties of blocking grain boundaries is impedance spectroscopy. This technique allows decomposing the overall *dc* resistance into contributions of the grain interior, the grain boundaries, and the electrodes.

Four BT powders with the same crystal structure and stoichiometry, but different average particle sizes, were used to investigate the influence of particle size on densification, microstructure of sintered ceramics, and their electrical properties, especially grain boundary resistance.

2. Experimental

$BaTiO_3$ powder (denoted as BT1), prepared by a conventional solid-state reaction between $BaCO_3$ (>99%) and TiO_2 (rutile, >99.8%) at 1100°C during 2 h, was used as the starting material. In order to investigate the influence of average particle size, and also powder de-agglomeration, on the shrinkage, microstructure, and electrical properties of BT ceramics, ultrasonication was performed in different time periods. The BT1 powder, with an average particle size of 1.4 μm, was dispersed in isopropanol and treated with high-intensity ultrasonication using a direct-immersion titanium horn (Sonics VCX-750, 20 kHz, 750 W; 85% amplitude, 2 s/1 s pulse). After 10, 60, and 180 min of ultrasonication BT powders with average particle size of 1.3 μm, 410 nm, and 64 nm were obtained, and denoted as BT2, BT3, and BT4, respectively. A more detailed description of the preparation of the initial barium titanate powder, its ultrasonication, and characteristics have been provided elsewhere [25].

The BT powders were uni-axially pressed into pellets (⌀ 4 mm and $h = 2$ mm) at 300 MPa. The average green density of the pellets was about 62% of theoretical density (T.D., 6.02 g/cm^3). The samples were sintered in a heating microscope (E. Leitz, Wetzlar, Germany) in order to determine the influence of average particle size on shrinkage behavior. The experiments were performed in air up to 1370°C, using a heating rate of 10°C/min, whereas the duration of isothermal sintering was 2 h. The changes in height (h) and diameter (d) of the samples durings the sintering process were recorded throughout the period of 4 h, at 10-min intervals. The density of the final ceramics was determined via picnometry.

The dielectric permittivity of BT ceramics was studied as a function of temperature. Dielectric measurements were done in a cooling regime, from 160 to 0°C. The measurements were performed between silver electrodes, in an air atmosphere, at 1 kHz using a Wayne Kerr Universal Bridge B224. The dielectric permittivity of BT ceramics was correlated to the average grain size, and, consequently, to the average particle size of BT powders. Additionally, the electric conductivity of BT samples was investigated by an *ac* impedance spectroscopy over the frequency range of 1 Hz–100 kHz using a Gamry EIS300 Impedance Analyzer, in cooling from 320 to 25°C; an applied voltage was 100 mV. The recorded impedance spectra were mathematically analyzed using the *ZView*2 software (version 2.6 demo).

The microstructure of the sintered ceramics was studied on previously thermally etched and gold coated surfaces by scanning electron microscopy (SEM model JSM 5300) operating at 30 kV. The obtained micrographs were used for the estimation of average grain size with a SemAfore digital slow scan image recording system (JEOL, version 4.01 demo).

3. Results and discussion

3.1. Powders Characteristics

In our previous article [25], we presented the results of a detailed examination of characteristics of the BT powders used in this study for the preparation of sintered ceramics. We examined average particle size, also, the extent and nature (soft or hard) of the agglomerates [25], because they have a strong bearing on sinterability and other related powder properties. Actually, powders have a tendency to form agglomerates, which cause grain growth during sintering, formation of microstructural defects, and/or microstress, thus disparaging the electrical properties of materials [28, 29].

Here, we emphasize that all of the used BT powders were highly crystalline, pure BT with tetragonal symmetry, which is especially important for achieving the best dielectric properties for BT ceramics [9]. The values of average particle size of the used BT powders are listed in Table 1.

3.2. Sintering

The heating microscope, as an excellent instrument for detailed quantitative studies of sintering kinetics [30–32], was used for *in situ* monitoring of the shrinkage processes.

Table 1.—Characteristics of the $BaTiO_3$ powders and ceramics sintered at 1370°C.

Sample	Average particle size (μm)	Average grain size (μm)	Density (% T.D.)	$\varepsilon_{r,\max}$	T_c (°C)	$T_{t/o}$ (°C)	γ	C' (×10^5°C)	R_{dc} at 25°C (GΩ)	R_g at 320°C (kΩ)	R_{gb} at 320°C (kΩ)
BT1	1.400	26	90.4	5920	108.2	21.1	1.25	2.06	2	50	187
BT2	1.300	25	91.9	6980	108.0	21.7	1.23	2.22	14	46	753
BT3	0.410	21	94.0	7520	106.6	22.1	1.35	3.50	56	75	937
BT4	0.064	18	97.8	7580	106.0	24.7	1.36	3.37	72	84	1650

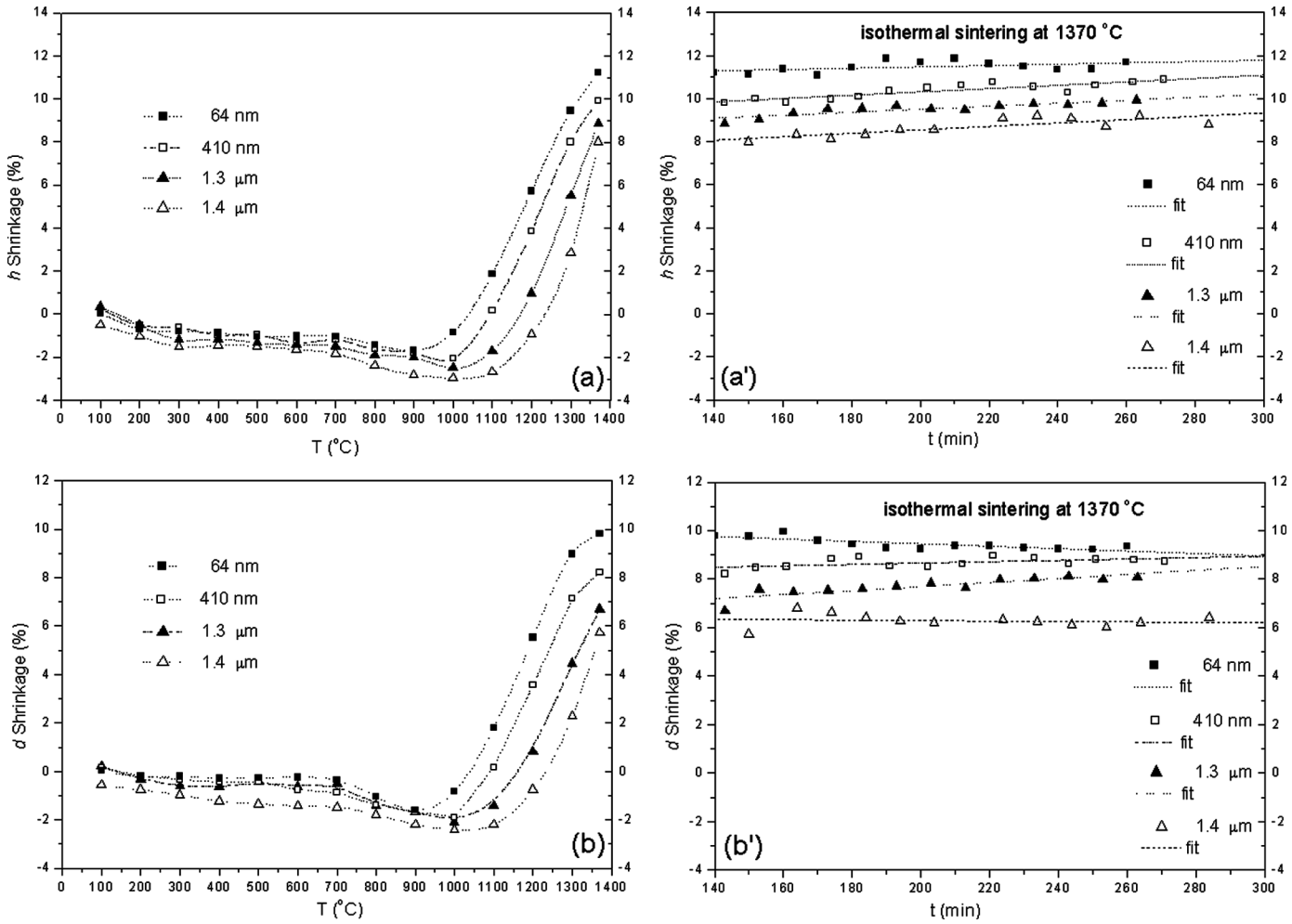

FIGURE 1.—Effect of sintering process on shrinkage: (a) nonisothermal axial shrinkage; (a′) isothermal axial shrinkage; (b) nonisothermal diameter shrinkage and (b′) isothermal diameter shrinkage.

Here, the sintering shrinkage of cylindrical compacts was recorded in axial (h) and radial (d) directions. From the experimental data for h and d recorded at 10-min time intervals during 4 h of sintering and using Eq. (1), the percentage of shrinkage was calculated for both the height and diameter:

$$\text{shrinkage } (\%) = \frac{\Delta l}{l_o} \times 100, \tag{1}$$

where Δl $(=l_o - l_i)$ denotes the difference between the initial value of height or diameter l_o at time t_o and the values l_i at time t_i. The calculated values of shrinkage were used for the determination of the samples' sintering behavior, including shrinkage anisotropy.

The densification of barium titanate samples is represented by shrinkage curves of the height and diameter of the bottom layer of the samples *versus* temperature, in non-isothermal sintering, Figs. 1(a) and (b), and vs. holding time, in isothermal sintering, Figs. 1(a′) and (b′). The shrinkage curves are relatively similar for all the investigated powders; they show that the main densification proceeds in the 900–1300°C temperature interval (during solid-state sintering), followed by a gentle parabolic increase of the shrinkage values during an isothermal sintering (slight densification proceeded with grain growth, probably due to the presence of a liquid phase). From Fig. 1(a), it can be seen that axial shrinkage begins at ~850°C for 64 nm-sized (BT4) powder, at 920°C for 410 nm-sized (BT3) powder, and near 1000°C for micro-sized (BT1 and BT2) powders. For nano-sized powder, shrinkage is especially intensive in the interval 900−1250°C, while for micro-sized powders this interval is shifted toward higher temperatures, ~1000–1300°C. Shrinkage is the most intensive for the BT4 (~12%) and the least intensive for BT1 powder (~9%).

The same densification trend is obtained for diameter shrinkage, Fig. 1(b). For the nano-sized powder, shrinkage begins at 900°C, whereby an almost complete densification is finished up to 1300°C, and the highest attained shrinkage is ~10%. Micro-sized powder (1.4 μm) shows intensive diameter shrinkage in temperature interval 1000–1370°C and the shrinkage reaches ~7%. During isothermal sintering, we observed a decreasing trend of d shrinkage,

Fig. 1(b′). This phenomenon is well known in the case of high shrinkage and high friction with the sintering substrate, when compacts exhibit different top vs. bottom shrinkage. The bottom drags on the sintering substrate while the top is unconstrained [33].

Moreover, it is noticed that axial shrinkage is larger than diametrical one ($\Delta h > \Delta d$), i.e., anisotropic densification occurs. A series of phenomenological hypotheses have been proposed as an explanation for the existence of shrinkage anisotropy, including the effect of gravity, residual stresses, varying density distribution in compacts, and preferred orientation of the crystal lattice [34]. In some recent articles, the origin of the anisotropic shrinkage was attributed to the orientation of elongated particles in the compacts in addition to the nonuniform particle packing density in uniaxially pressed compacts [35, 36]. A larger sintering shrinkage in the h direction than in the d direction occurs when elongated particles align with their longest axis perpendicular to the direction of uniaxial pressing within the plane parallel to the direction of uniaxial pressing and randomly oriented within the plane normal to the uniaxial pressing [36].

Generally, we find that nano-sized BT powder shows the highest value of shrinkage in both axial and diameter directions compared to micro- and submicro-sized powders. Moreover, sintering of the nano-sized powder occurs at a lower temperature interval.

Different shrinkage behaviors of BT1-BT4 samples can be explained by different densification of powder compacts containing more or less agglomerated particles. One of the explanations for the retardation of the densification in samples containing agglomerated particles is the existence of porosity in the green body [32–37]. Different pore types in the initial compacts, with wide variation in pore curvature, have different free surface energies and thus lead to an overall different driving force for sintering in dense ceramics [33].

A convenient way of quantifying shrinkage anisotropy of sintered materials is the calculation of shrinkage anisotropy factor k [32]. In cylindrical compacts, k determines the extent of shrinkage anisotropy relating axial (height) and diametrical shrinkage. The shrinkage anisotropy was calculated using Eq. (2)

$$\text{anisotropy factor} = k = \frac{\Delta d}{\Delta h} = \frac{d_o - d_i}{h_o - h_i}, \tag{2}$$

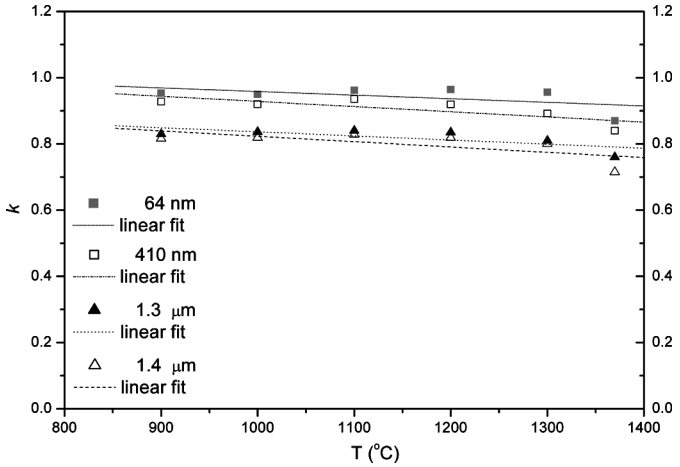

FIGURE 2.—Shrinkage anisotropy factor k, with respect to powders particle size.

where d_o and d_i denote the diameter, whereas h_o and h_i denote the height, at initial time t_o and at time t_i, respectively.

The values of k, calculated according to the Eq. (2), are presented in Fig. 2 as a function of sintering temperature (from 900 to 1370°C). It can be observed that the anisotropy factor for all samples is $k < 1$. Here, the shrinkage anisotropy can be explained by the use of BT powders consisting of anisotropy crystallites elongated in (200) direction [25], as well as by their nonuniform packing during uni-axially pressing. Besides, with the decrease of average particle size, k strives to 1, which indicates that the use of BT powders with lower average particle size and softer agglomerates leads to a more uniform package during uni-axial pressing, whereas shrinkage tends to be isotropic. Obviously, average particle size, their morphology, as well as the nature of agglomerates were repercussive onto the densification process and anisotropy factor.

Figures 3(a) and (b) shows the microstructure of sintered BT ceramics produced from micro- (BT1) and nano-sized (BT4) powders, respectively. The microstructure of typical polycrystalline ceramics, with an interconnected network of large angular grains can be observed. Each

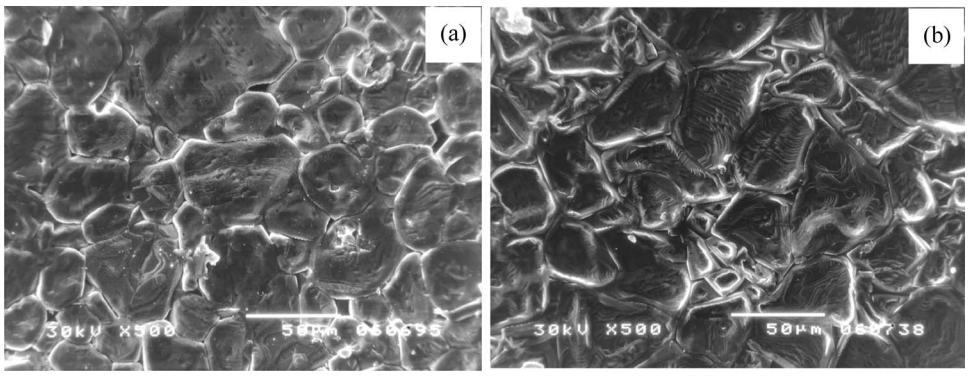

FIGURE 3.—Microstructures of $BaTiO_3$ ceramics, sintered at 1370°C during 2 h, prepared from BT powders with average particle size: (a) 1.4 μm and (b) 64 nm.

grain is surrounded by randomly oriented neighbors, closely adhering at the grain boundaries. Rounded grain corners imply that a liquid-phase-assisted mechanism has been operating during sintering at 1370°C. For all sintered ceramics the densification is high, and ranging from 90 (for BT1) to 98% of T.D. (for BT4). There is a difference in grains shape and size between ceramics prepared from micro- and nano-sized powders. Platelike grains, with a stress free surface and average size of $G_{av} = 26\,\mu m$ grow from powder BT1, Fig. 3(a), while the reduction of the average particle size of BT powder to 64 nm leads to a slight decrease in the average grain size of the final ceramics down to $G_{av} = 18\,\mu m$, Fig. 3(b). Moreover, high sintering temperature (and/or prolonged time) produces compressive residual stress in BT4 ceramic, inducing a layered grain texture where most layers are oriented with their *c*-axes normal to the sample surface. Therefore, nano-scaled barium titanate powder produces high-density ceramics with smaller average grain size.

Here, we call attention to the fact that during sintering processes grains grow up to 50 μm in size. These results are in agreement with the previously published ones, which show that even nano-crystalline powder has a tendency to form agglomerates, which causes grain growth during sintering [28, 29]. Besides, as it is shown, almost complete densification is finished up to 1300°C. Further annealing produced slight densification proceeded with grain growth. In addition, the activation energy of the grain boundary migration in BT is quite small, resulting in increased grain growth during the final stage of sintering [38].

Grain growth usually occurs due to the material transport by volume diffusion, surface diffusion or evaporation-condensation process. During the evaporation-condensation process, spiral growth can be induced at structural imperfections in ceramics like as screw dislocations, micro-twins, stacking faults etc. [33–40]. In Fig. 4 we show microstructure of the ceramic prepared from BT4 powder ($d_{50} = 64$ nm); the presence of spiral-concentric grains is evident. Therefore, the existence of spiral growth mechanism can be a reliable explanation for a large grain growth in the sintered BT ceramics [41]. Moreover, this indicates a significant role of the evaporation-condensation process during final stages of sintering.

The average grain size and percent of theoretical density are given in Table 1.

3.3. Electrical Measurements

The dielectric properties of ceramics prepared from BT powders with different average particle size are relatively similar, Fig. 5. They exhibit a sharp maximum in permittivity at T_c with clear evidence of permittivity peak ascribed to the tetragonal to orthorhombic phase transition ($T_{t/o}$). The decrease in average particle size causes a slight shift of T_c toward lower and $T_{t/o}$ toward higher temperatures (Table 1). Furthermore, $\varepsilon_{r,\max}$ clearly increases with the reduction of the powder's average particle size, from 5920, for the ceramic prepared from BT1 powder, up to 7580, for the ceramic prepared from BT4 powder. Elsewhere, a similar finding was explained by the microstructure of sintered ceramics [42], which can be applied in this case, too. Namely, a slight shift of T_c was provoked by the decrease of G_{av} from 26 to 18 μm, while the increase of $\varepsilon_{r,\max}$ was caused by the increases of density from 90.4–97.8% of T.D.

Moreover, Kinoshita and Yamaji [42] have showed that ε_r strongly depends on the grain size in ferroelectric

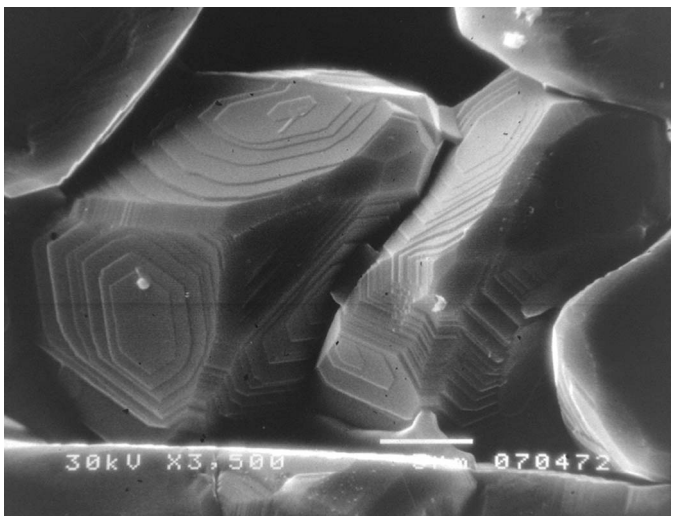

FIGURE 4.—Microstructure with spiral-concentric grain growth phenomenon. $BaTiO_3$ with average particle size of 64 nm sintered at 1370°C during 2 h.

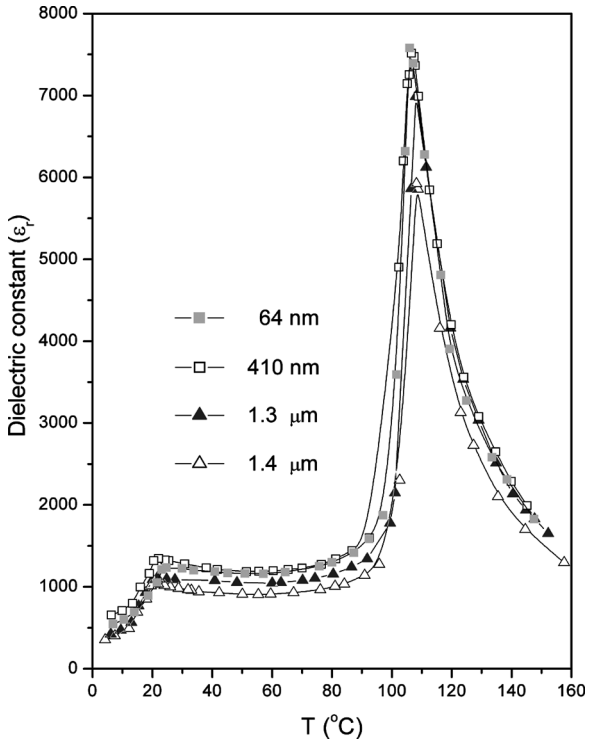

FIGURE 5.—The temperature dependence of dielectric constant of $BaTiO_3$ ceramics sintered at 1370°C during 2 h, with respect to powders particle size.

state, while it is almost independent on the grain size in paraelectric state, where ε_r follows the Curie–Weiss law.

It can be emphasized that the symmetry reduction at the cubic-tetragonal (i.e., paraelectric-ferroelectric) phase transition depends on the grain size and stress effects, and therefore is greatly influenced by the microstructure of the sintered material [21]. Generally, size and stress effects may induce a shift of T_c to lower temperatures, the broadening of the phase transition temperature range, and a change in dielectric permittivity. The manner in which these effects occur depends on the order of the phase transition. Martirena and Burfoot [43] proposed the following empirical relation (3) for the temperature (in the range above Curie temperature) variation of ε during the phase transition from normal ferroelectric (λ phase transition) to diffuse phase transition:

$$\frac{1}{\varepsilon_r} - \frac{1}{\varepsilon_{r,\max}} = \frac{(T - T_{\max})^{\gamma}}{C'}, \tag{3}$$

where $T_{\max}$ is the temperature of dielectric constant maximum, C' is modified Curie–Weiss constant, and γ is the critical exponent which can vary from 1 for normal to 1–2 for diffuse phase transition. Parameters γ and C' were calculated from linear functional dependence: $\ln(1/\varepsilon_r - 1/\varepsilon_{r,\max})$ vs. $\ln(T - T_{\max})$, at temperatures above $T_{\max}$ (Fig. 6), and are given in Table 1. Evidently, calculated values for γ are similar for all the examined samples, while C' is slightly changed from $2.06 \cdot 10^5$ to $3.37 \cdot 10^5$ °C. These values are almost independent on grain size, which means that the behavior of ε_r is not influenced by grain size above $T_{\max}$. Hence, in the paraelectric state ε_r follows the Curie–Weiss law.

Such a difference between paraelectric and ferroelectric states indicates that internal stress plays an important role in grain-size effects because it does not grow in the cubic phase but develops when $BaTiO_3$ ceramics are cooled below T_c [42].

The permittivity of BT ceramics measured at the fixed frequency of 1 kHz (Fig. 5) gives information relevant to their practical applications; however, a large amount of additional information could be obtained by varying frequency. For instance, polycrystalline materials may show a variety of frequency-dependent effects associated with heterogeneities, such as grain boundaries or surface layers, as well as with intrinsic properties of the grains of the materials under consideration. In such cases, fixed-frequency measurements not only give restricted amount of information but in addition, any interpretation of fixed-frequency data may be ambiguous [44, 45]. By *ac* impedance measurements in a wide range of frequencies, and at various temperatures, one may determine individual values of various resistance components, such as grain boundary and grain (bulk) resistance and permittivity, and examine their dependence on temperature. Usually, the complex impedance diagram, in the so-called Nyquist presentation (the plot of imaginary Z'' vs. real Z' impedance, with the frequency ω as an independent parameter) of a sintered, low-conducting material between blocking electrodes, consists of two adjacent semicircles, ending at the origin of coordinate system at infinite frequency. For sintered BT ceramics, the low-frequency semicircle of the impedance spectra is attributed to the grain boundary impedance, whereby the one corresponding to higher frequencies is attributed to intra-grain (bulk) response [44, 46–49]. The grain interior and grain boundary resistance may be read as the diameter of high-frequency and low-frequency arcs, respectively.

In this study, in addition to single frequency data shown in Fig. 5, the electrical properties of BT ceramics in the temperature range of 25–320°C were examined by *ac*

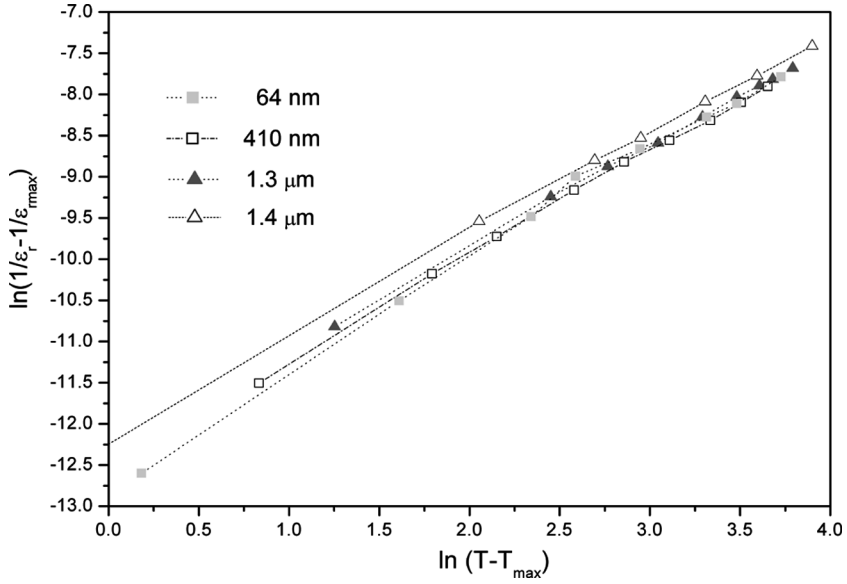

FIGURE 6.—Plots of $\ln(1/\varepsilon_r - 1/\varepsilon_{r,\max})$ vs. $\ln(T - T_{\max})$ for $BaTiO_3$ samples sintered at 1370°C during 2 h, with respect to powders particle size.

impedance spectroscopy. The resistance and capacitance elements were determined by fitting an appropriate equivalent circuit to the impedance data. Here, the aim of impedance measurements was to determine the influence of grain size, i.e., microstructure (and consequently the influence of the powder's particle size) on the sample resistivity, which was possible because all the samples had equal dimensions and the same chemical composition (i.e., stoichiometry).

Figue 7 shows the impedance spectra of the sintered BT ceramics at three representative temperatures. Obviously, the shape of Nyquist plots depends on temperature. At room temperature [Fig. 7(a)], the shape of Nyquist plot follows a straight line with a large slope indicating the insulating behavior of the samples. The *dc* resistance (*dc*–frequency-independent resistance [46]) of the samples measured at room temperature was estimated, by *ZView* 2 software, to be in the range of $2-72 \cdot 10^9\ \Omega$. Thus, at room temperature, the impedance of the BT ceramics is too high. Due to Hirose and West [44] the room temperature resistivity of BT ceramics depends mainly on the microstructural development associated with grain growth. Only the data obtained above T_c, when the grain boundary resistance experiences a drop by four orders of magnitude (from 10^{10} to $10^6\ \Omega$) provide more useful information. Furthermore, in order to separate grain and grain boundary contributions, BT samples were heated up to 320°C. The low frequency arc was not found at <200°C, which may be due to the effect of electrode relaxation process overlapping with the grain boundary relaxation process. However, with increase in the temperature (≥230°C, Fig. 7(b)) impedance spectra for all the samples contained two semicircles (arcs). It can be seen From Fig. 7(c) that the amplitude of the high-frequency arc of impedance spectra for BT samples having different grain sizes does not vary significantly with the decrease in grain size. The high-frequency arc can thus be ascribed to the bulk resistance (R_b). The amplitude of the low-frequency arc increases with decreasing grain size, and is ascribed to grain boundary resistance (R_{gb}).

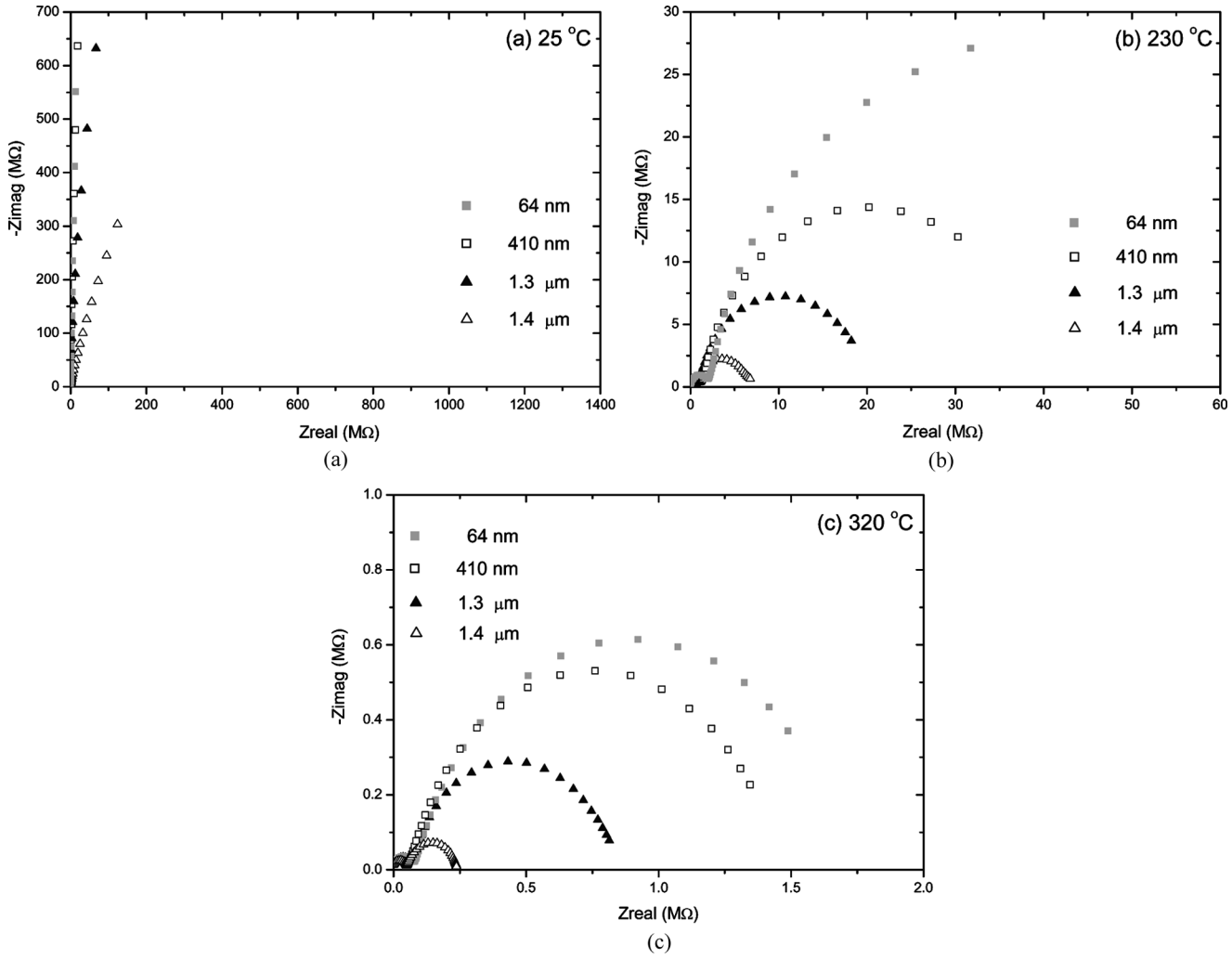

FIGURE 7.—Complex impedance spectra of the sintered $BaTiO_3$ ceramics at three representative temperatures, with respect to starting powders average particle size.

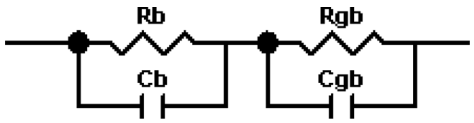

FIGURE 8.—Equivalent circuit used to represent the electrical properties of sintered $BaTiO_3$ ceramics.

The experimental data of *ac* impedance measurements may be alternatively presented in terms of equivalent circuit. There is no *a priori* method to find the best equivalent circuit. For a given data set, it is always possible to find more than one equivalent circuit model that can fit the data. Usually, the complex impedance diagram in the form of two adjacent arcs has been modeled using an equivalent circuit consisting of two parallel resistance-capacitance (*RC*) elements connected in series [44–50]. To represent the impedance properties of BT ceramics at temperatures above the ferroelectric-paraelectric transition T_c, shown in Figs. 7(b, c), an equivalent circuit consisting of two parallel *RC* elements connected in series, presented in Fig. 8, was proved to be the best among possible equivalent circuits. The high-frequency arc corresponds to R_bC_b response and low-frequency arc corresponds to $R_{gb}C_{gb}$ response. The spectrum clearly indicates a combination of bulk and grain boundary impedances connected in series. The impedance Z^* for this circuit can be described with Eq. (4) [44]:

$$Z^* = \left[R_b^{-1} + j\omega C_b\right]^{-1} + \left[R_{gb}^{-1} + j\omega C_{gb}\right]^{-1}. \quad (4)$$

After fitting, the R_b and R_{gb} resistances were read as the diameter of high- and low-frequency arc, respectively, and their values are presented in Table 1. It can be noticed that the values of bulk resistance R_b are nearly independent on the average particle size. On the contrary, the grain boundary resistance R_{gb} is influenced by the average particle size of the starting powder. Obviously, the grain boundary resistance increases with the decrease of BT powder average particle size, which is due to repercussion on the ceramic's microstructure, i.e., average grain size and density. It can be noticed that the overall grain boundary resistance increases with the decrease in the grain size, due to the increase in the number of boundaries per unit thickness [51]. R_b and R_{gb} also decrease with an increase in temperature.

The grain boundary is ferroelectric just like the grains, but its impedance is modified by either air gaps surrounding the grain-to-grain contacts or by high-impedance electrical inhomogeneity in the region of the necks between grains [44]. At temperature above T_c, the capacitance of air gaps increasingly dominates.

Grain boundaries are often laterally inhomogeneous (i.e., "imperfect") in the sense that ideally conducting as well as totally insulating interface regions are present. To give two examples: (i) solid grain boundary phases often only partially wet the grains, establishing a diminishing grain-to-grain contact, and (ii) nano-pores along grain boundaries can cause an imperfect contact between two grains. In such cases, insulating layer partly separates neighboring grains. Consequently, bulk resistance may be significantly higher than the ideal bulk resistance [52].

Imperfect contacts (lateral inhomogeneities) between grains cause current constriction in the grains. This leads to an apparent grain boundary semicircle, whose diameter is purely bulk-dependent [52].

4. CONCLUSION

The correlation between densification, microstructure, and electrical properties (dielectric permittivity and grain boundary resistance) of BT ceramics prepared from $BaTiO_3$ powders with different average particle size (1.4 μm, 1.3 μm, 410 nm, and 64 nm) was investigated.

Shrinkage was found to be very sensitive to the barium titanate powder average particle size. The reduction of the average particle size ensures improved densification of BT powders. Shrinkage begins at 850°C for nano-sized (64 nm) powder, at 920°C for submicro sized (410 nm) powder while the micro-sized ones (1.3 and 1.4 μm) begin to shrink at 1000°C. Furthermore, the sintering curves were shifted to lower temperatures with decreasing average particle size of the powders.

A decrease in the average particle size of the initial powder leads to a reduction of the average grain size of the sintered ceramics. Ceramics prepared at 1370°C during 2 h using powder with an average particle size of 1.4 μm, consisted of grains enlarged up to 50 μm, while the average particle size of 64 nm yielded the final grains reaching an average size of 18 μm.

The microstructure of BT ceramics significantly influences their electrical properties. A reduction of the average grain size and an increase in density promote an increase in both dielectric constant and grain boundary resistivity.

It is shown that the powder's average particle size and/or the size of agglomerates have limiting influence on the grain size in the final ceramic. It is also shown that electrical characteristics of BT ceramics primarily depend on the average grain size of the sintered samples. All investigated properties, including dielectric constant and grain boundary resistivity, increase with a decrease in average grain size. It should be emphasized that the electrical characteristics of the sintered ceramics are very sensitive to ceramic density, grain size, and the shape of grain boundaries. Therefore, fine-particles BT powder is desirable for achieving a higher grain boundary resistivity.

Furthermore, impedance spectroscopy shows that the electrical behavior of grain boundaries depends on the ceramic's microstructure and consequently on the starting powder's average particle size.

Finally, it may be emphasized that uniform nano-sized BT powder with tetragonal crystal structure, prepared by a solid-state reaction followed by high-intensity ultrasonication during 3 hours, is suitable for the preparation of dense ceramics with good electrical properties.

ACKNOWLEDGMENTS

The Ministry of Science and Technological Development of the Republic of Serbia provided financial support under Grant No. 142006. The authors would like to thank Prof. N. Cvjetićanin and Prof. D. Janaćković for their kind help during the experimental work.

References

1. Gablenz, S.; Damm, C.; Müller, F.W.; Israel, G.; Rössel, M.; Röder, A; Abicht, H.-P. Preparation and characterization of core-shell structured TiO_2-$BaCO_3$ particles. Solid State Sciences **2001**, *3*, 291–299.
2. Phule, P.P.; Rispud, S.H. Review: Low-temperature synthesis and processing of electronic materials in the BaO–TiO_2 system. Journal of Materials Science **1990**, *25*, 1169–1183.
3. Anliker, M.; Brugger, H.R.; Känzig, W. Study of fine powders ferroelectrics II: Barium titanate $BaTiO_3$. Helvetica Physica Acta **1954**, *27*, 99–124.
4. Tsurumi, T.; Sekine, T.; Kakemoto, H.; Hoshina, T.; Nam, S.-M.; Yasuno, H.; Wada, S. Evaluation and statistical analysis of dielectric permittivity of $BaTiO_3$ powders. Journal of the American Ceramic Society **2006**, *89*, 1337–1341.
5. Garcia, R.E.; Carter, W.C.; Langer, S.A. The effect of texture and microstructure on the macroscopic properties of polycrystalline piezoelectrics: application to barium titanate and PZN–PT. Journal of the American Ceramic Society **2005**, *88*, 750–757.
6. Uchino, K.; Sadanaga, E.; Hirose, T. Dependence of the crystal structure on particle size in barium titanate. Journal of the American Ceramic Society **1989**, *72*, 1555–1558.
7. Song, Y.-L.; Liu, X.-L.; Zhang, J.-Q.; Zou, X.-Y.; Chen, J.-F. Rheological properties of nanosized barium titanate prepared by HGRP for aqueous tape casting. Powder Technology **2005**, *155*, 26–32.
8. Ying, K.-L.; Hsieh, T.-E. Sintering behaviors and dielectric properties of nanocrystalline barium titanate. Materials Science and Engineering B **2007**, *138*, 241–245.
9. Xu, H.; Gao, L. Tetragonal nanocrystalline barium titanate powder: Preparation, characterization, and dielectric properties. Journal of the American Ceramic Society **2003**, *86*, 203–205.
10. Zhao, Z.; Buscaglia, V.; Viviani, M.; Buscaglia, M.T.; Mitoseriu, L.; Testino, A.; Nygren, M.; Jonhsson, M.; Nanni, P. Grain-size effects on the ferroelectric behavior of dense nanocrystalline $BaTiO_3$ ceramics. Physical Review B **2004**, *70*, 024107-1–024107-8.
11. Buscaglia, V.; Viviani, M.; Buscaglia, M.T.; Nanni, P.; Mitoseriu, L.; Testino, A.; Stytsenko, E.; Daglish, M.; Zhao, Z.; Nygren, M. Nanostructured barium titanate ceramics. Powder Technology **2004**, *148*, 24–27.
12. Park, Z.H.; Shin, H.S.; Lee, B.K.; Cho, S.H. Particle size control of barium titanate prepared from barium titanyl oxalate. Journal of the American Ceramic Society **1997**, *80*, 1599–1604.
13. Xu, H.; Gao, L.; Guo, J. Hydrothermal synthesis of tetragonal barium titanate from barium chloride and titanium tetrachloride under moderate conditions. Journal of the American Ceramic Society **2002**, *85*, 727–729.
14. Pfaff, G. Sol-gel synthesis of barium titanate powders of various compositions. Journal of Materials Chemistry **1992**, *2*, 591–596.
15. Ritter, J.J.; Roth, R.S.; Blendell, J.E. Alkoxide precursor synthesis and characterization of phases in the barium-titanium oxide system. Journal of the American Ceramic Society **1986**, *69*, 155–162.
16. Tsay, J.-D.; Fang, T.-T. Effects of temperature and atmosphere on the formation mechanism of barium titanate using the citrate process. Journal of the American Ceramic Society **1996**, *79*, 1693–1696.
17. Milošević, O.B.; Mirković, M.K.; Uskoković, D.P. Characteristics and formation mechanism of $BaTiO_3$ powders prepared by twin-fluid and ultrasonic spray-pyrolysis methods. Journal of the American Ceramic Society **1996**, *79*, 1720–1722.
18. Kwon, S.-G.; Choi, K.; Kim, B.-I. Solvothermal synthesis of nano-sized tetragonal barium titanate powders. Materials Letters **2006**, *60*, 979–982.
19. Beauger, A.; Moutin, J.C.; Niepce, J.C. Synthesis reaction of metatitanate $BaTiO_3$. Journal of Materials Science **1983**, *18*, 3543–3550.
20. Balaž, P.; Briančin, J.; Bastl, Z.; Medvecky, L.; Šepelak, V. Properties of mechanochemically pretreated precursors of doped $BaTiO_3$ ceramics. Journal of Materials Science **1994**, *29*, 4847–4851.
21. Pavlović, V.P.; Nikolić, M.V.; Nikolić, Z.; Branković, G.; Živković, LJ.; Pavlović, V.B.; Ristić, M.M. Microstructural evolution and electric properties of mechanically activated $BaTiO_3$ ceramics. Journal of the European Ceramic Society **2006**, *27*, 575–579.
22. Uskoković, D.P.; Samsonov, G.V.; Ristić, M.M. *Activated Sintering*; Publ. Intern. Inst. for the Science of Sintering: Belgrade, 1974.
23. Pavlović, V.P.; Nikolić, M.V.; Pavlović, V.B.; Labus, N.; Živković, Lj.; Stojanović, B.D. Correlation between densification rate and microstructure evolution of mechanically activated $BaTiO_3$. Ferroelectrics **2005**, *319*, 75–85.
24. Thakur, O.P.; Feteira, A.; Kundys, B.; Sinclair, D.C. Influence of attrition milling on the electrical properties of undoped-$BaTiO_3$. Journal of the European Ceramic Society **2007**, *27*, 2577–2589.
25. Marković, S.; Mitrić, M.; Starčević, G.; Uskoković, D. Ultrasonic de-agglomeration of barium titanate powder. Ultrasonics Sonochemistry **2008**, *15*, 16–20.
26. Rout, S.K.; Panigrahi, S.; Bera, J. Study of electrical properties of Ni-doped $SrTiO_3$ ceramics using impedance spectroscopy. Bulletin of Materials Science **2005**, *28*, 275–279.
27. Greuter, F.; Blatter, G. Electrical properties of grain boundaries in polycrystalline compound semiconductors. Semiconductor Science and Technology **1990**, *5*, 111–137.
28. Ferkel, H.; Hellmig, R. Effects of nanopowders deagglomeration on the densities of nanocrystalline ceramics green body and their sintering behavior. Nanostructured Materials **1999**, *11*, 617–622.
29. Groza, J.R. Nanosintering. Nanostructured Materials **1999**, *12*, 987–992.
30. Skorohod, V.; Olevsky, E.; Shtern, M. Continuum theory of sintering of the porous bodies: model and application. Int. J. Sci. Sinter. **1991**, *23*, 79–91.
31. Boccaccini, A.R. Sintering of glass matrix composites containing Al_2O_3 platelet inclusions. Journal of Materials Science **1994**, *29*, 4273–4278.
32. Boccaccini, A.R.; Adell, V.; Cheeseman, C.R., Conradt, R. Use of heating microscopy to assess sintering anisotropy in layered glass metal powder compacts. Advances in Applied Ceramics **2006**, *105*, 2532–3540.
33. German, R.M. *Sintering Theory and Practice*; John Wiley & Sons, Inc.: New York, Chichester, Brisbane, Toronto, Singapore, 1996.
34. Mitkov, M.; Exner, H.E.; Petzow, G. Orientation of pore structure in loose and stressed carbonyl iron and its influence on shrinkage anisotropy. Ristic, M.M. (Ed.); In: Sintering: New Developments, Materials Science Monographs Vol. 4, Elsevier: Amsterdam, Oxford, New York, 1979; 90–98.

35. Shui, A.; Uchida, N.; Uematsu, K. Origin of shrinkage anisotropy during sintering for uniaxially pressed alumina compacts. Powder Technology **2002**, *127*, 9–18.
36. Shui, A.; Kato, Z.; Uchida, N.; Uematsu, K. Sintering deformation caused by particle orientation in uniaxially and isostatically pressed alumina compacts. Journal of the European Ceramic Society **2002**, *22*, 311–316.
37. Boccaccini, A.R.; Conradt, R. Isotropic shrinkage of platelet containing glass powder compacts during isothermal sintering. International Journal of Inorganic Materials **2001**, *3*, 101–106.
38. Frey, M.H.; Payne, D.A. Grain size effect on structure and phase transformation for barium titanate. Physical Review B **1996**, *54*, 3158–3168.
39. Kingery, W.D.; Bowen, H.K.; Uhlmann, D.R. *Introduction to Ceramics*, 2nd Ed.; John Wiley & Sons: New York, Chichester, Brisbane, Toronto, Singapore, 1976.
40. Uskoković, D.P.; Palmour III, H.; Spriggs, R.M. (Eds.) *Science of Sintering: New Directions for Materials Processing and Microstructural Control*; Plenum Press: New York and London, 1989.
41. Schmelz, H.; Meyer, A. The evidence for anomalous grain growth below the eutectic temperature in $BaTiO_3$ ceramics. Ceramic Forum International **1982**, *59*, 436–440.
42. Kinoshita, K.; Yamaji, A. Grain-size effects on dielectric properties in barium titanate ceramics. Journal of Applied Physics **1976**, *47*, 371–373.
43. Martirena, H.T.; Burfoot, J.C. Grain-size and pressure effects on the dielectric and piezoelectric properties of hot-pressed PZT-5. Ferroelectrics **1974**, *7*, 151–152.
44. Hirose, N.; West, A.R. Impedance spectroscopy of undoped $BaTiO_3$ ceramics. Journal of the American Ceramic Society **1996**, *79*, 1633–1641.
45. Sinclair, D.C.; West, A.R. Impedance and modulus spectroscopy of semiconducting $BaTiO_3$ showing positive temperature coefficient of resistance. Journal of Applied Physics **1989**, *66*, 3850–3856.
46. Macdonald, J.R. (Ed.) *Impedance Spectroscopy*; John Wiley & Sons: New York, Chichester, Brisbane, Toronto, Singapore, 1987.
47. Morrison, F.D.; Sinclair, D.C.; West, A.R. Characterization of lanthanum-doped barium titanate ceramics using impedance spectroscopy. Journal of the American Ceramic Society **2001**, *84*, 531–538.
48. V'yunov, O.I.; Kovalenko, L.L.; Belous, A.G.; Belyakov, V.N. Oxidation of reduced Y-doped semiconducting barium titanate ceramics. Inorganic Materials **2005**, *41*, 93–100.
49. Belous, A.; V'yunov, O.; Kovalenko, L.; Makovec, D. Redox processes in highly yttrium-doped barium titanate. Journal of Solid State Chemistry **2005**, *178*, 1367–1375.
50. West, A.R.; Sinclair, D.C.; Hirose, N. Characterization of electrical materials, especially ferroelectrics, by impedance spectroscopy. Journal of Electroceramics **1997**, *1*, 65–71.
51. Jurado, R.J.; Colomer, M.T.; Frade, J.R. Electrical characterization of $Sr_{0.97}Ti_{1-x}Fe_xO_{3-\delta}$ by complex impedance spectroscopy: I, Materials with low iron contents. Journal of the American Ceramic Society **2000**, *83*, 2715–2720.
52. Fleig, J. The influence of non-ideal microstructures on the analysis of grain boundary impedances. Solid State Ionics **2000**, *131*, 117–127.